

A Noninvasive Method for Analysis of Epileptogenic Brain Connectivity



Mark E. Pflieger¹ and Bassam A. Assaf²

¹Source Signal Imaging, Inc., San Diego, CA

²University of Illinois College of Medicine at Peoria, Peoria, IL



Presented at the American Epilepsy Society 2004 Annual Meeting, New Orleans, December 6, 2004. Abstract in *Epilepsia* 45 (Suppl. 7): 70-1.

Correspondence:

Mark E. Pflieger

2323 Broadway, Suite 102

San Diego, CA 92102 USA

email: mep@sourcesignal.com

phone: +1-619-234-9935 ext 15

<http://www.sourcesignal.com/>

Introduction¹

Source analyses of interictal and ictal scalp EEG may implicate the involvement of *multiple* cerebral regions. Fast neuroelectric activity from candidate regions may be estimated on a macroscopic spatial scale using a *local* source estimator such as regional activity estimation (REGAE; [7], [8]). From such derived time series, we aim to assess ***dysfunctional connections*** between brain regions around the times of interictal or ictal onset discharges by measuring ***causal influences***. We have been developing a new approach, “causal source analysis” of scalp EEG, to study cerebral connectivity and influences among regions involved with epileptogenicity. Here we describe our general approach, and apply it to ictal onset EEG for a patient with temporal lobe epilepsy. (See [3], [4], & [9] for related studies at this meeting.) Our measure of causal influence is based on the concept of ***time-lagged causally conditional mutual information*** ([5], [6]), which has *linear* (ICCM) and *nonlinear* (*n*CCMI) variants. This study utilizes the linear measure, which is based on *Gaussian* statistics. Given two brain ROIs A and B, CCMI is the amount of statistical information about the later state of B obtained by knowing of A’s earlier state, after having discounted information that could be obtained via B’s earlier state and A’s later state.

¹ We devised two improvements in methodology after submitting the original abstract (*Epilepsia* 45(Suppl. 7): 70-1): an *adaptive* REGAE algorithm, and a *statistical test*. The methods and results reported here have been updated to reflect our current state of the art.

Overview of Causal Source Analysis Procedure

Select ROIs; // 8 ROIs were used in this illustration: See Fig. 1.

For each ROI: Apply adaptive REGAE to multi-channel EEG to obtain “current configuration” vector time series; // See Figs. 2 & 3

High-pass filter for independent sampling via λ constraint (below);
// See Fig. 4 (high-pass filtered ROI vector time series)

Iterate the following K times:

Select N random times subject to a no-closer-than- λ constraint;

For each ROI pair:

For each time lag: // (The following are described below)

Compute linear causally conditional mutual information (LCCMI);

Obtain p -values via randomization;

Accumulate p -values (for average);

Average p -value = Accumulator/ K ;

Make lag graphs; // See Fig. 5

Obtain 1-sided interaction indices & derived indices; // See Table 1

Make causal network diagram; // See Fig. 6.

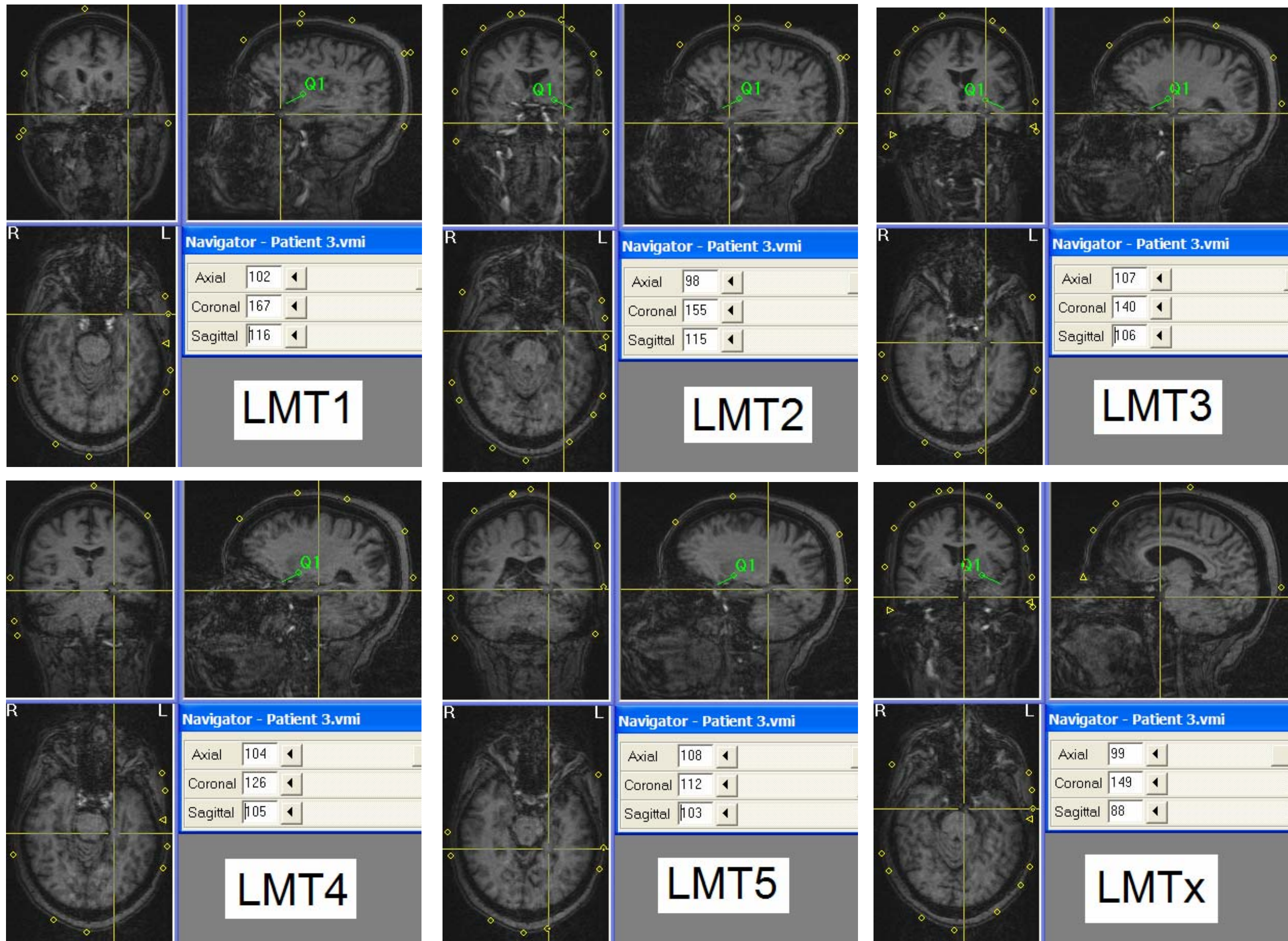
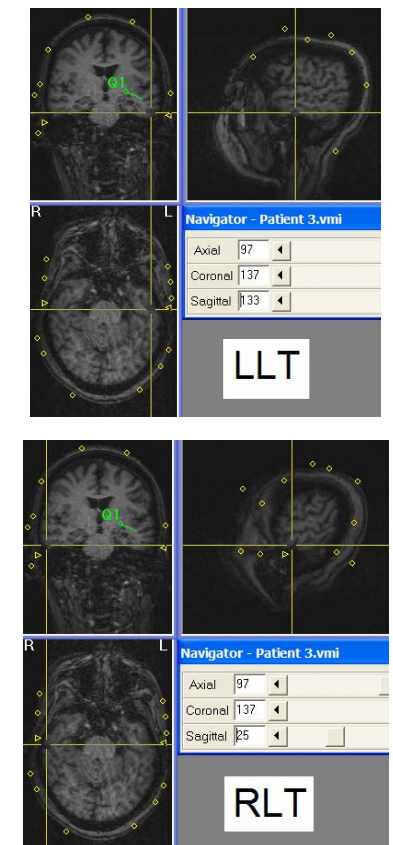


Fig. 1. Centers of 8 ROIs chosen for causal interaction analysis are shown at crosshairs (radiological convention). LMT1 – LMT5 make up a “virtual strip” of left medial temporal lobe locations, ranging from anterior (LMT1) to posterior (LMT5) with about 15 mm separation. LMTx is the location of maximum activity found via adaptive REGAE scanning. RLT is a local minimum in right lateral temporal lobe, and LLT is its approximate mirror image. “Q1” indicates the location and orientation of an ECD that was fit in the frequency domain to a prominent peak at 3.41 Hz.



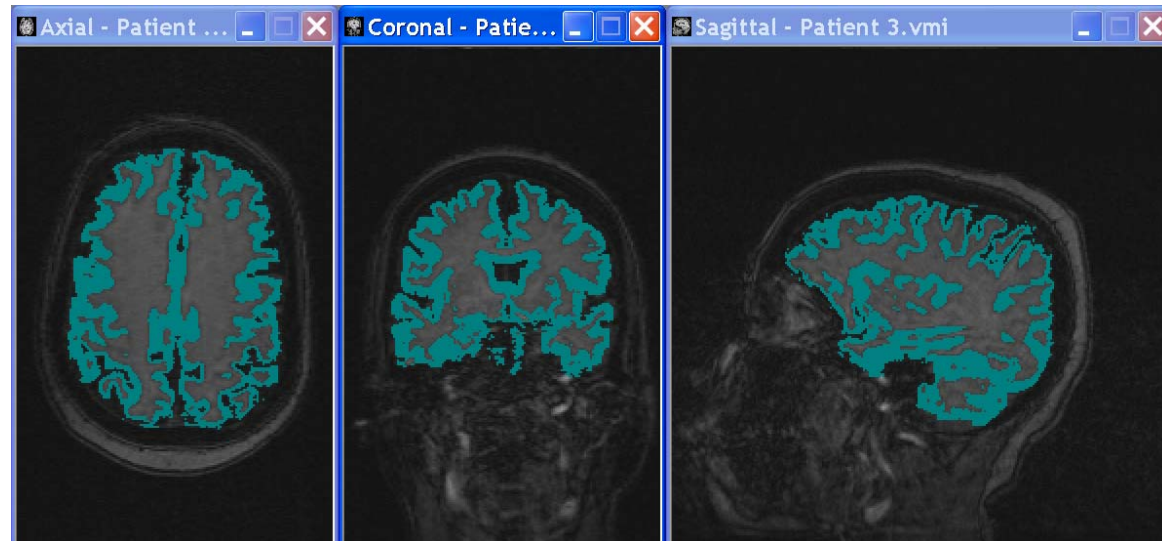


Fig. 2. The source space used in this illustration consisted of 4176 locations packed no closer than 5 mm throughout brain gray matter. 3 orthogonal dipole elements were placed at each location. Using a criterion of packing no closer than 15 mm, 240 of these locations were selected for REGAE scanning.

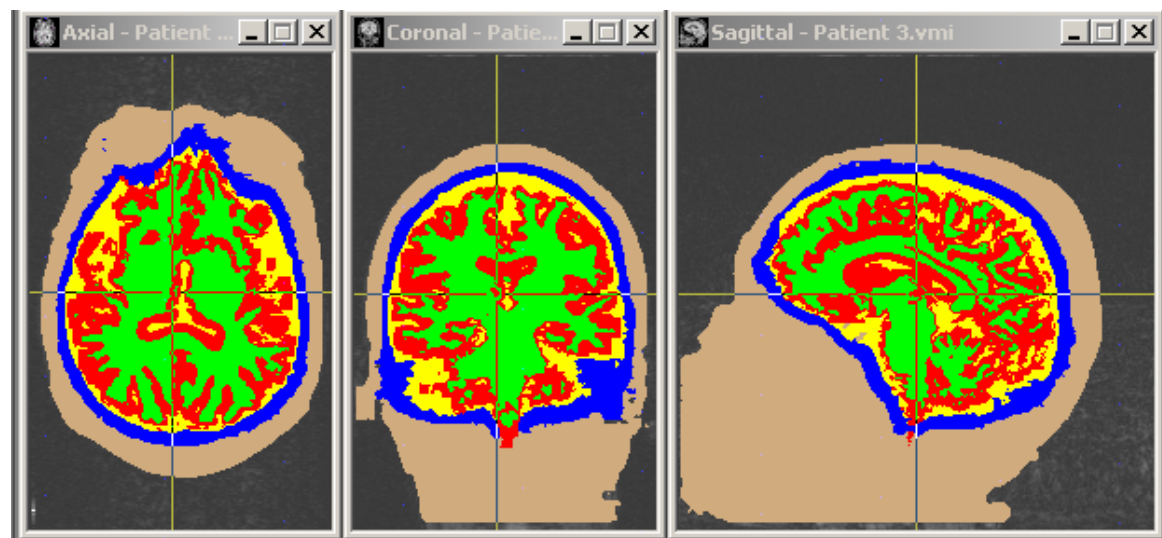


Fig. 3. A finite element method (FEM) head model was constructed from the tissue parcellation shown at left (white matter, gray matter, CSF, bone, skin). This was tiled with a tetrahedral mesh, and a forward operator was computed via an efficient FEM solver.

Regional activity estimation (REGAE) was applied for each ROI to estimate “configurational states” of within-ROI activity (i.e., spatial configurations of within-ROI current flow). REGAE is a local bioelectric source estimation method for deriving ROI vector time series from scalp EEG (or MEG) data ([7], [8]). As a *local* method, REGAE does not attempt to solve a global inverse problem. Instead, an estimator (“virtual intracranial electrode” on a macroscopic spatial scale) is derived independently for each ROI. The method seeks to balance a tradeoff between *spatial resolution*, as measured by the spread of a region around a location in gray matter, and *discriminability* between intra-ROI and extra-ROI activity, as measured by the area under a suitably constructed receiver operator characteristic curve (AUROC). Specific resolution/discriminability characteristics depend principally on the ROI location in the brain, the EEG electrode configuration, and the source space model of gray matter. Spatial resolution is permitted to vary across brain regions in order to match discriminability characteristics. For example, deep brain locations have lower spatial resolution (i.e., larger regional spread) in comparison with superficial locations. REGAE utilizes a gray matter source space model (Fig. 2) and a volume conductor model of the head (Fig. 3). **Adaptive REGAE** utilizes, in addition, an estimate of the covariance statistics of the scalp EEG. During seizure, the covariance statistics change markedly.

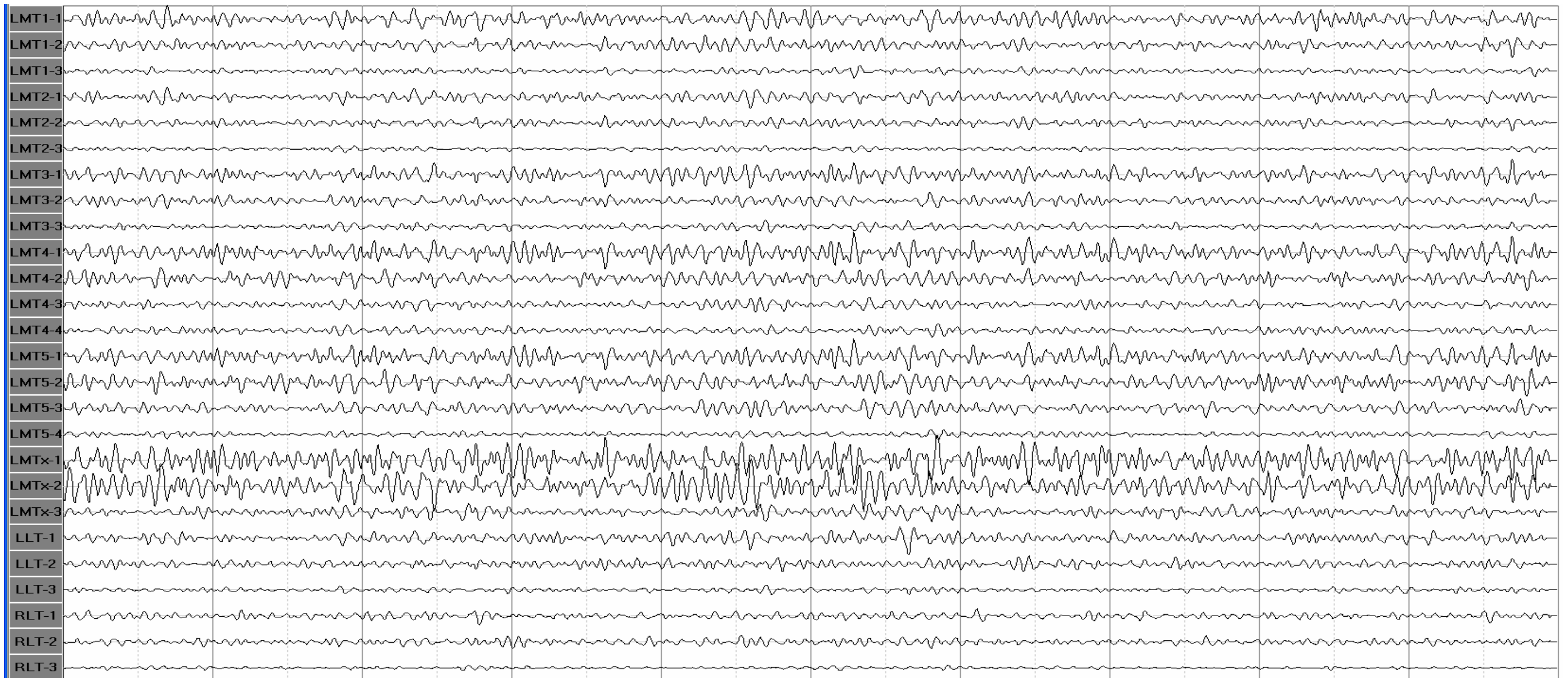


Fig. 4. 8 Hz highpass filtered (see rationale below) regional time series for one of two 10 s seizure EEG samples, derived via adaptive regional activity estimation (REGAE). “Adaptive” here means that (a) the 57-channel EEG data were projected to a 40-dimensional nonsingular subspace obtained via SVD of the seizure covariance matrix (estimated from all 20 s of data) and (b) the theoretical ROI covariance was forward-projected to the same subspace and “whitened” via reciprocals of the seizure covariance principal values. The estimator dimension d for each ROI was set by allowing a 10:1 ratio of maximum to minimum projected activity; this produced $d=3$ for all ROIs except LMT4 and LMT5, for which $d=4$. Note that estimated ROI activity tends to decrease across successive dimensions. LMTx is the region with greatest estimated activity.

Time-lagged causal conditional mutual information. Given two brain regions A and B in a context C , the formulation for *causal CMI* is $I(A(t), B(t+s) | A(t+s), B(t), C(t), C(t+s))$, where $A(t)$ denotes the state of region A at time t , etc., and s is a time lag. *Ordinary mutual information (MI)* $I(A(t), B(t+s))$ quantifies *predictability* of B 's later state from A 's earlier state. However, to approach *causality* in a provisional sense, some conditions are specified as *confounds*, i.e., as enablers of *noncausal* predictability. For example, a region C may drive both A and B ; or it may mediate them; etc. Aside from such third regions, note that A 's later state and B 's earlier state are listed as confounds to discount three pathways of noncausal predictability made possible when A and B are instantaneously correlated, e.g., via artifactual estimator cross-talk, or actual volume conduction: (i) $A(t)$ correlates with $B(t)$, which could predict $B(t+s)$ via internal dynamics; (ii) likewise, $A(t)$ could predict via internal dynamics $A(t+s)$, which correlates with $B(t+s)$; and (iii) $A(t)$ correlates with $B(t)$, which could predict via genuine causality in the opposite direction $A(t+s)$, which correlates with $B(t+s)$. *Linear CMI*, employed here, is closely related to partial correlation.

Nonparametric statistical test for linear causal CMI. To obtain p -values for observed values of linear causal CMI, we applied a new randomization test described in reference [6]. However, we devised a new technique to work with short time samples (20 s total): *To enable independent sampling* of the EEG with points no closer than 200 ms, we 8 Hz bandpass filtered the ictal EEG data (which removed a considerable portion of the total seizure EEG power; but we accepted this tradeoff in order to do the statistics). We computed CMI and p -values; and we iterated this procedure 100 times, averaging the p -values (shown below).

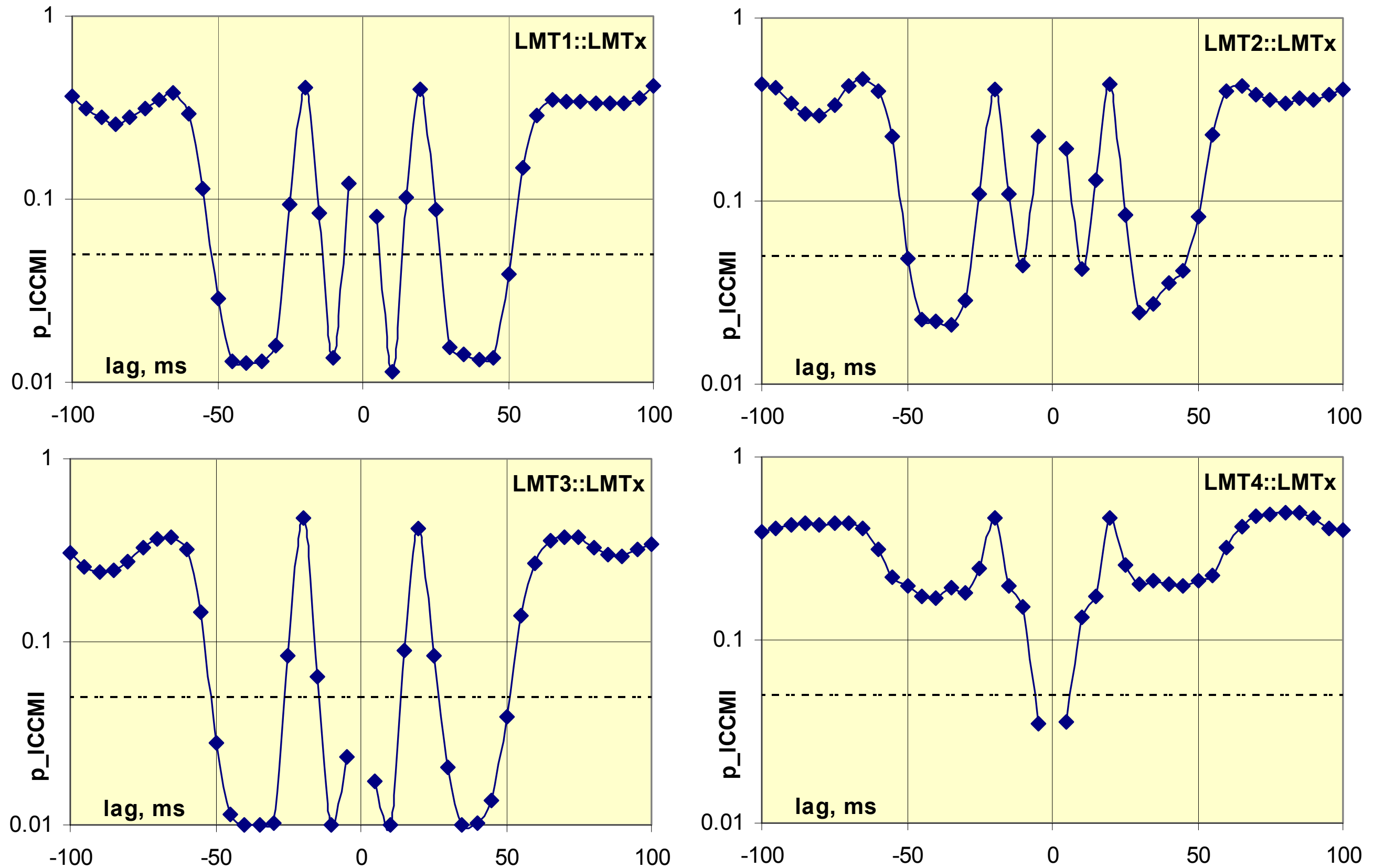


Fig. 5a. We computed CMI for all 28 ROI pairs; only 7 pairs achieved significance at the level of 0.05 (dashed line). Note log scale for p -values.

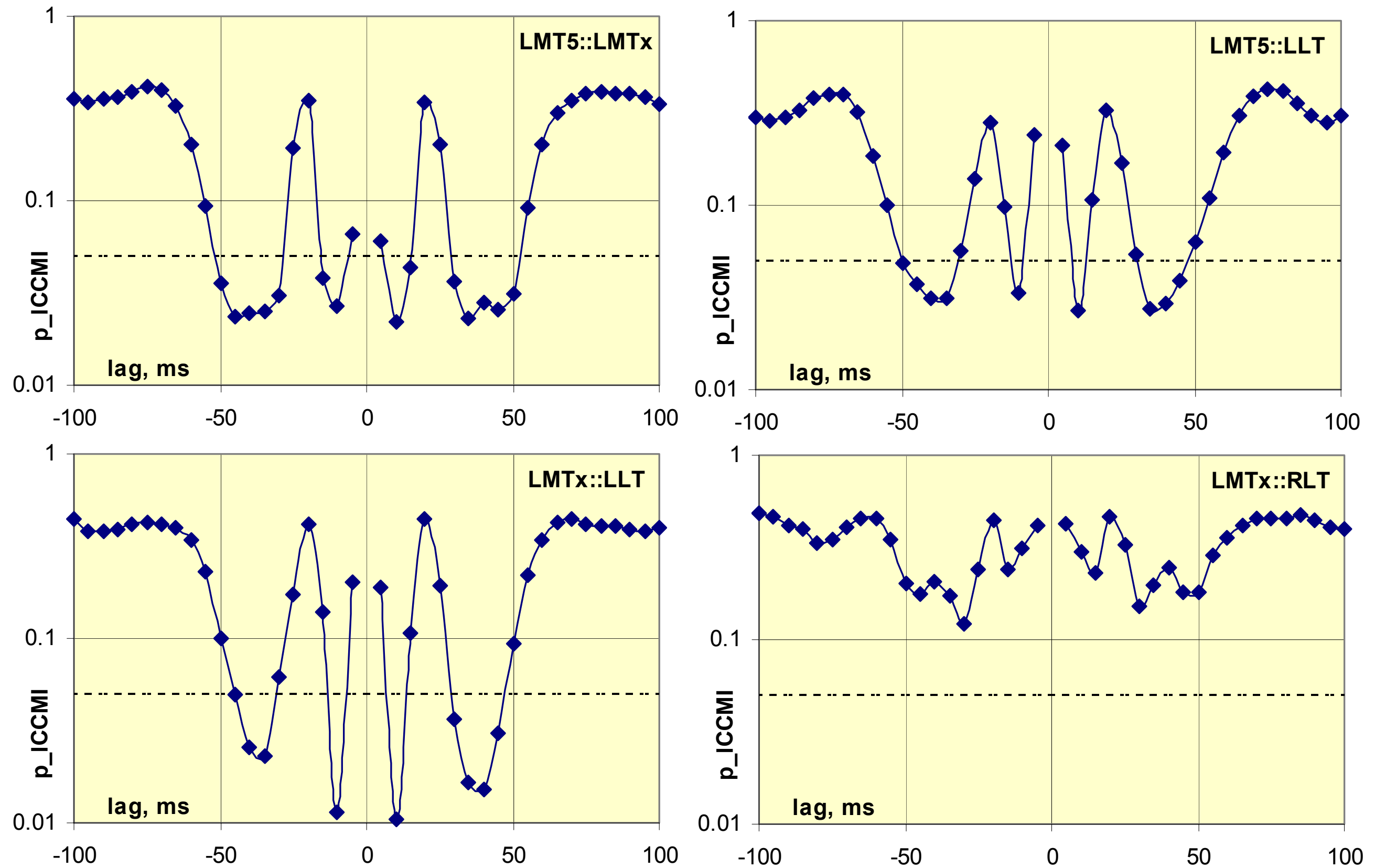


Fig 5b. Positive lag refers to the first named ROI. Twenty-one pairs did not achieve significance, and one pair (LMTx::RLT) is shown as an example.

| Table 1 | | 1-sided interaction indices | | Derived indices | |
|----------------|-------------|-----------------------------|-----------|-----------------|-------------------|
| <i>ROI1</i> | <i>ROI2</i> | <i>I1</i> | <i>I2</i> | <i>I1+I2</i> | $(I2-I1)/(I1+I2)$ |
| LMTx | LMT1 | 6.760 | 7.083 | 13.84 | 2.3% |
| LMTx | LMT2 | 2.005 | 3.183 | 5.118 | 23.0% |
| LMTx | LMT3 | 8.299 | 9.201 | 17.50 | 5.2% |
| LMTx | LMT4 | 0.334 | 0.360 | 0.694 | 3.7% |
| LMTx | LMT5 | 3.758 | 3.904 | 7.662 | 1.9% |
| LMTx | LLT | 2.938 | 4.665 | 7.603 | 22.7% |
| LMT5 | LLT | 1.668 | 1.999 | 3.667 | 9.0% |

Table 1 contains “1-sided interaction indices” and other indices derived from these. The “*I1*” column is the sum of $-\log(p)+\log(0.05)$ across all negative lags for which $p<0.05$. Likewise, the “*I2*” column is the sum across positive lags. Thus, *I1* measures the extent to which *ROI1* leads *ROI2*, and *I2* measures the reverse. The derived index ***I1+I2* measures total interactivity**, and **$(I2-I1)/(I1+I2)$ measures interaction asymmetry**, expressed as a percent. Positive asymmetry indices indicate that $I2 > I1$.

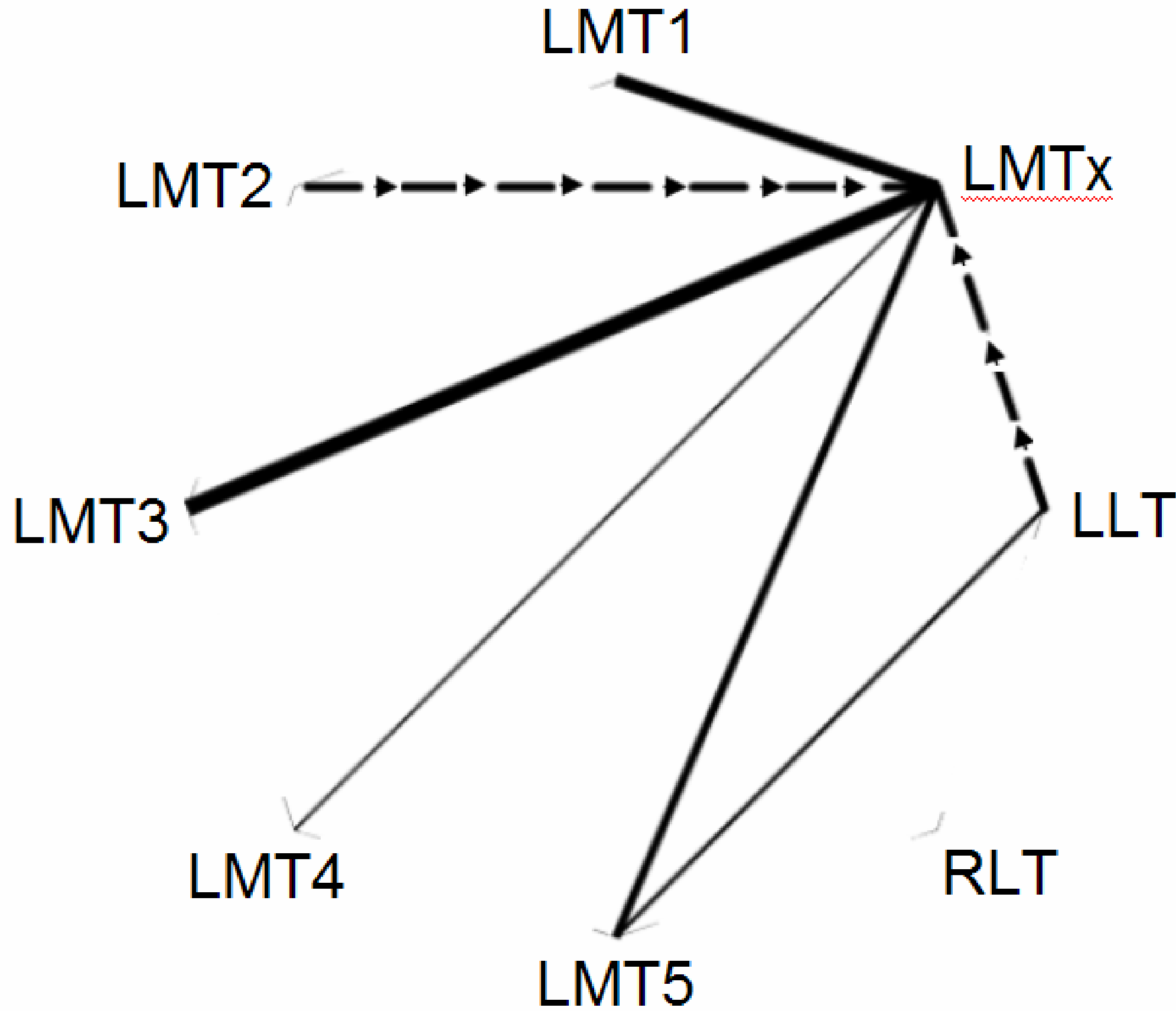


Fig. 6. The causal network diagram at left depicts the results of Table 1. Line thicknesses reflect total interactivity. Arrows point toward the causally subordinate node for interactions with $>|20\%$ asymmetry.

Discussion

The ROI that reflected greatest r.m.s. seizure activity, *LMTx*, was also the dominant “hub” of the causal network diagram. Because *p*-values are scale independent, there was no a priori bias in favor of this result. **All significant interactions detected from these seizure samples were predominantly symmetric**, seeming to imply mutual causality between brain regions involved in seizure activity, soon after seizure onset. However, closer inspection uncovered a small but consistent asymmetry: All asymmetry indices for *LMTx* are positive, indicating that the other regions are somewhat causally dominant. In the absence of actual asymmetry, the probability of 6 all-positive asymmetry indices is $(0.5)^6 = 0.016$. This suggests that **the putative seizure focus (*LMTx*) may be hyperexcitable, i.e., over-sensitive to inputs from other regions [1]**. High interactivity in both 10 ms and 35-45 ms time lag zones is consistent with previous findings that there are fast and slow neuronal conduction systems in the temporal lobe [2]. The consistency in the high interaction findings among the ROIs supports the face validity of this analysis. In addition, the areas that demonstrate high interactions in this example (*LMTx*, *LMT3*, and *LMT1*) are located in the mesial temporal and anterior basal/temporal tip regions, which are the areas likely involved in the seizure activity in this patient, who has a classical mesial temporal lobe epilepsy by history and mesial temporal sclerosis visible on MRI, which indicate that the seizures are most likely originating from the mesial temporal lobe. (This is a preliminary report on an ongoing study.)

References²

- [1] Bernard C, Anderson A, Becker A, Poolos NP, Beck H, Johnston D (2004): Acquired dendritic channelopathy in temporal lobe epilepsy. *Science* 305:532-5.
- [2] Holsheimer J, Lopes da Silva FH (1989): Propagation velocity of epileptiform activity in the hippocampus. *Exp Brain Res* 77(1):69-78.
- [3] Hunter JD, Reimer J, Hanan DM, Hecox KE, Towle VL (2004): Locating subdural electrodes in CT images using 3-D surface reconstruction. *Epilepsia* 45(Suppl. 7): 300. *This meeting, #2.235.*
- [4] Jackson GD, Waites AB, Briellmann RS, Labate A, Masterson R, Abbott DF (2004): Functional connectivity identifies an epileptogenic network in idiopathic generalized epilepsy. *Epilepsia* 45(Suppl. 7): 300-1. *This meeting, #2.236.*
- [5] Pflieger ME (2003): Time-lagged causal information: A new metric for effective connectivity analysis. HBM 2003, New York City.²
- [6] Pflieger ME (2004): Statistical assessment of linear and nonlinear causal interactions. *NeuroImage* 22(Suppl. 1) CD-ROM.²
- [7] Pflieger ME, Assaf BA, Greenblatt RE, Jiang H (2003): A regional scanning approach for localizing sources of epileptiform EEG. *Epilepsia* 44(Suppl. 9): 257.²
- [8] Pflieger ME, Assaf BA, Greenblatt RE, Yazeji, Carine E, Mohamed F (2002): Imaging EEG in temporal lobe regions of interest: Effects of head model and electrode density on spatial resolution. *Neurology* 58 (Suppl 3): A141-2.²
- [9] Shah A, Rivera M, Ismail D, Vazquez JG, Agarwal R, Blumenfeld H (2004): Neocortical spread of limbic kindled seizures. *Epilepsia* 45(Suppl. 7): 25. *This meeting, #1.036.*

Acknowledgment: Supported by NIBIB 1 R43 EB000614.

² References [5] – [8] are available online at <http://www.sourcesignal.com/papers.html>.